Investigation of Resistive Wall Mode Stabilization Physics in High Beta Plasmas Using Applied Non-axisymmetric Fields in NSTX*

A.C. SONTAG 1), S.A. SABBAGH 1), W. ZHU 1), J.E. MENARD 2), R.E. BELL 2), J.M. BIALEK 1), M.G. BELL 2), D.A. GATES 2), A.H. GLASSER 3), B.P. LEBLANC 2), K.C. SHAING 4), D. STUTMAN 5), K.L. TRITZ 5)

1) Columbia University, New York, NY, USA
2) Princeton Plasma Physics Laboratory, Princeton University, Princeton, NJ, USA
3) Los Alamos National Laboratory, Los Alamos, NM, USA
4) University of Wisconsin, Madison, WI, USA
5) John Hopkins University, Baltimore, MD, USA

e-mail contact of main author: asontag@pppl.gov

Abstract: The National Spherical Torus Experiment (NSTX) offers an operational space characterized by high-beta (β_t = 39%, β_N > 7, $\beta_N/\beta_N^{\text{no-wall}}$ > 1.5) and low aspect ratio (A > 1.27) to leverage the plasma parameter dependences of RWM stabilization and plasma rotation damping physics giving greater confidence for extrapolation to ITER. Significant new capability for RWM research has been added to the device with the commissioning of a set of six non-axisymmetric magnetic field coils, allowing generation of fields with dominant toroidal mode number, n, of 1-3. These coils have been used to perform low-frequency MHD spectroscopy of the RWM. As expected by theory, the resonant response of the RWM peaks when applied n = 1 fields propagate in the direction of plasma rotation. Modification of plasma rotation profiles shows that rotation outside q = 2.5 is not required for passive RWM stability and there is large variation in the RWM critical rotation at the q = 2 surface, both of which are consistent with distributed dissipation models. An electromagnetic model based on tearing mode interaction with non-axisymmetric fields does not reproduce the observed RWM critical rotation for stability. Increased ion collisionality is correlated with decreased critical rotation. The measured decrease of the plasma toroidal angular momentum profile in experiments is compared to calculations of non-resonant drag torque based on the theory of neoclassical toroidal viscosity. Quantitative agreement between experiment and theory is found when the effect of toroidally trapped particles is included.

1. Introduction

Generating fusion power most efficiently in future magnetic fusion devices such as ITER requires that long wavelength magnetohydrodynamic (MHD) instabilities be stabilized at high plasma stored energy compared to the energy of the confining magnetic field. Research on the stabilization of MHD modes in existing high performance fusion devices is therefore important for the optimal success of ITER. The National Spherical Torus Experiment (NSTX) [1] offers a high performance operational space characterized by high-beta ($\beta_t \equiv 2\mu_0\langle p\rangle/B_0^2$ = 39%, $\beta_N \equiv 10^8\langle\beta_t\rangle aB_0/I_p$ > 7, $\beta_N/\beta_N^{\text{no-wall}}$ > 1.5) and low aspect ratio (A > 1.27) to leverage the plasma parameter dependences of RWM stabilization and associated physics, giving greater confidence for extrapolation to ITER. Here, p is the plasma pressure, B_0 is the vacuum toroidal field at the plasma geometric center, and I_p is the plasma current.

The pressure-driven ideal MHD kink-ballooning mode requires stabilization for a fusion plasma to reach and maintain high β_t. When destabilized, the mode rapidly grows on the short Alfvén timescale (typically microseconds in magnetic fusion plasmas) and generally leads to significant loss of plasma confinement and current disruption. This mode rotates along with the bulk plasma rotation and with modest rotation can be stabilized by a conducting wall sufficiently close to the plasma boundary. [2] The presence of the conducting wall leads to the existence of the resistive wall mode (RWM) [3,4] that can also disrupt plasma confinement, but grows on the much slower current decay time of the

conducting wall, τ_{wall}. RWM destabilization can occur when β_N exceeds the value at which ideal MHD kink-ballooning modes become unstable, $\beta_N^{no\text{-}wall}$.

The RWM can be passively stabilized by plasma toroidal rotation, ω_ϕ, flowing through the mode [3,5]. Passive stabilization alone is presently thought to be insufficient in ITER, due to a relatively slow plasma rotation [6]. In such cases, RWM passive stabilization can be supplemented with active stabilization by externally applied magnetic fields. Therefore, it is important to understand the characteristics of RWM passive stabilization, including the critical plasma toroidal rotation required to maintain stability, Ω_{crit}, to best determine the degree of RWM active stabilization required for a fusion device. Equally important is understanding the physical mechanisms responsible for plasma momentum dissipation to determine how the favorable plasma rotation can be sustained and maximized, or how the plasma rotation profile might be controlled in future tokamaks.

Significant new capability to study and diagnose the RWM and the physics of plasma rotation damping has been added to NSTX with the commissioning of a set of six non-axisymmetric magnetic field coils. This paper describes experiments that utilize this coil to study the behavior of passively stabilized, high β_N plasmas, to examine the magnitude and profile shape of ω_ϕ required for RWM passive stabilization, and how Ω_{crit} depends on plasma parameters. In addition, applied non-axisymmetric fields are used both to control plasma rotation in these experiments and to quantitatively evaluate physics models responsible for plasma momentum dissipation.

The non-axisymmetric field coil on NSTX has most recently been used for its primary purpose - to actively stabilize the resistive wall mode. The results of these experiments are reported elsewhere (see Ref. [7]) and have been submitted as a separate post-deadline paper to this conference.

2. Non-axisymmetric coil and RWM control hardware

NSTX is equipped with 48 toroidally segmented copper conducting plates, covered with carbon tiles facing the plasma, that provide kink-ballooning mode stabilization (Fig. 1). These plates are arranged symmetrically in four toroidal rings, two above and two below the device midplane. The segments are independently connected to the stainless steel vacuum vessel by high resistance supports. Detection of the RWM is primarily made by magnetic loops measuring the radial, B_r, and poloidal, B_p, flux located at each of the plates closest to the midplane, the B_r sensors mounted between the carbon tiles and the copper shells and the B_p sensors mounted a few centimeters below each plate. The sensors are instrumented to detect modes with frequencies up to 2.5 kHz. The signals are processed to measure toroidal mode number, n, up to 3.

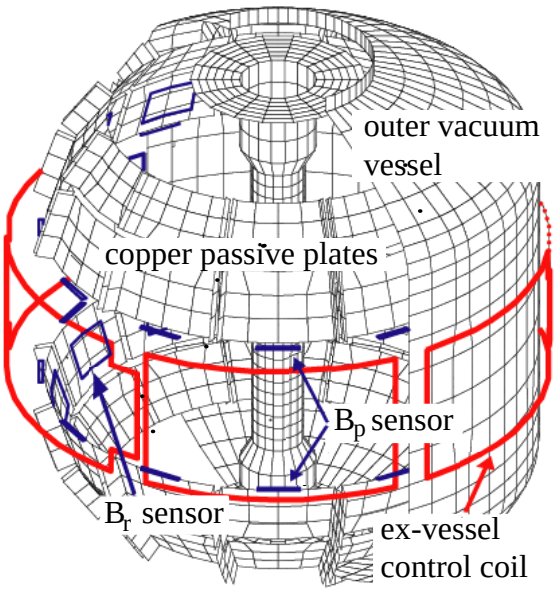

Fig. 1: Diagram of NSTX showing internal B_p and B_r sensors, passive stabilizers, and ex-vessel control coils.

The non-axisymmetric coil set is comprised of six control coils located at the outboard midplane (Fig. 1). Each coil has two turns, spans approximately 60 degrees of toroidal angle, and is located outside, but closely coupled to the device vacuum vessel. To date, these coils have been connected in diametrically-opposed, anti-series pairs that allow generation of odd parity n = 1 and 3

magnetic fields. Each coil pair is powered by an independent switching power amplifier capable of operation up to 3.3 kA at 7.5 kHz. This current corresponds to 10-15G of n = 1 midplane radial field at the q = 2 surface. The fields generated by these coils can be used to reduce or amplify static and dynamic error fields, control ω_ϕ, and actively control the RWM. The configuration of a midplane non-axisymmetric coil with conducting structure between the coil and the plasma is similar to proposed active stabilization system designs for ITER.

3. The RWM at high β_N and resonant field amplification

The characteristics of the unstable RWM at low A have been documented in NSTX. Early work determined that the RWM eigenfunction is ballooning in nature with the largest perturbation on the outboard side and that the mode effectively couples to the passive stabilizing plates [8]. The presence of large error fields resulted in unstable RWM growth soon after β_N exceeded $\beta_N^{no\text{-}wall}$, indicating reduced passive stabilization in this condition [9]. Subsequent error field reduction resulted in a much larger stabilized operating space with $\beta_N/\beta_N^{no\text{-}wall}$ up to 1.5 at the highest β_N values [10]. Maintaining high toroidal rotation across the entire profile leads to passive RWM stability. [11] Unstable RWMs with toroidal mode number up to three were observed. [10]

Study of RWM marginal stability conditions, and further characterization of the mode is provided by analysis of the *stable* RWM. Analysis of weakly damped RWMs in DIII-D [5] have shown that plasmas with $\beta_N > \beta_N^{no\text{-}wall}$ exhibit a pressure-driven amplification of applied non-axisymmetric fields (resonant field amplification, or RFA). [12] The RFA magnitude is defined as the ratio of the plasma-induced field amplitude (measured field minus applied vacuum field) to the applied vacuum field amplitude. This amplification is important, as it leads to an increase in plasma rotation damping that scales as the square of the field magnitude, δB. An initial investigation was carried out using two of the six ex-vessel coils, determining that the RFA increased with β_N with a magnitude in the range expected from DIII-D studies. [10] Further studies of the stable RWM have now been conducted using the full non-axisymmetric coil set, allowing toroidally propagating n = 1 applied fields to be used to determine RWM characteristics by active, low-frequency MHD spectroscopy. Results from this analysis are shown in Fig. 2 and are similar to results found in DIII-D. [13] The RFA magnitude generated by the stable n = 1 RWM is dependent on the frequency and the toroidal propagation direction of the applied n = 1 field. As expected by RWM theory, the RFA magnitude peaks when the applied field propagates in the direction of the plasma flow. Analysis of the RFA using a single mode model of the RWM yields a natural mode rotation frequency of 45 Hz.

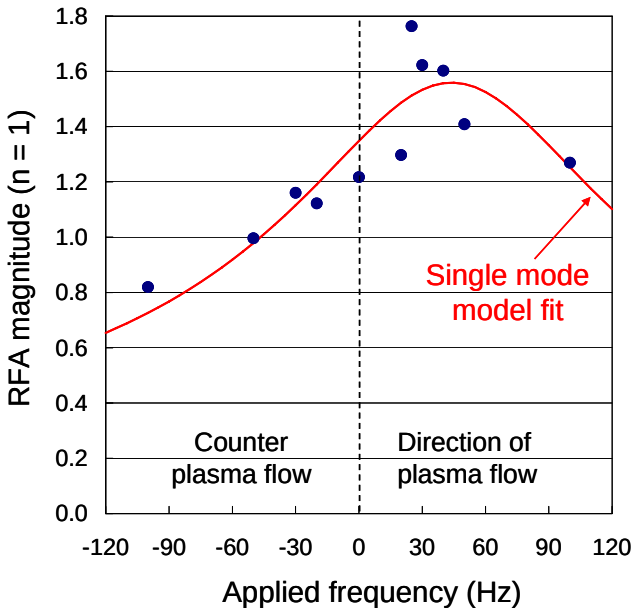

Fig. 2 RFA magnitude of stable n = 1 RWM vs. applied n = 1 non-axisymmetric field frequency.

An independent determination of the natural mode rotation frequency was performed by applying a non-propagating n = 3 AC field to a plasma near RWM marginal stability conditions to cyclically reduce ω_ϕ below Ω_{crit}. VALEN-3D [14] calculations of RWM stability and rotation using experimental equilibrium

reconstructions [15] are consistent with the average measured n = 1 RWM mode rotation value of about 50 Hz in these experiments. An n = 1 RWM growth time of 3.7 ms was measured as the mode became unstable, also consistent with these calculations.

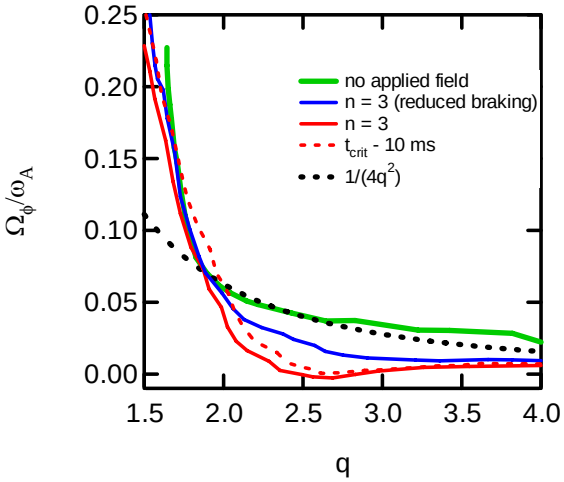

Fig. 3: Ω_{crit} variation for 3 discharges and the change in rotation over 10 ms for the strongest n = 3 braking case.

4. Passive stabilization and critical rotation profile

The RWM can be passively stabilized by plasma rotation flowing through the relatively stationary mode, coupled to an energy dissipation mechanism that leads to stability. [3,16,17] RWM stability therefore depends on both $\beta_N/\beta_N^{no\text{-}wall}$ and ω_ϕ. The RWM marginal stability point is probed by producing variations of both the magnitude and shape of the ω_ϕ profile. Past research has focused on the rotation at a particular rational q surface (typically q = 2 or 3) as a scalar figure of merit in determining the RWM stability boundary. Toroidal rotation and the toroidal coupling of poloidal harmonics can cause the dissipation to shift away from the rational surfaces, leading to a distributed form of dissipation [6] that is consistent with the overall rotation profile being more important for stability determination rather than rotation at a single rational surface. NSTX research has examined the dependence of Ω_{crit} on q, and found previously that maintaining the entire toroidal rotation profile above the value $\omega_C = \omega_A/4q^2$ led to sustained wall-stabilized operation [11]. This criteria, used as a benchmark for the present studies, is consistent with energy dissipation through coupling the RWM to the lowest branch of the Alfvén continuum and toroidal inertia enhancement [18].

Modification of ω_ϕ using externally applied non-axisymmetric fields has been performed to determine the significance of the rotation profile in passive stabilization. Fig. 3 shows the marginally stable toroidal rotation profile for three discharges. The q profile monotonically increases from the core to the edge, as determined from equilibrium reconstructions using internal field pitch angle data. The plasma with the highest rotation at high q has no external field applied, and largely matches the critical rotation profile, ω_C. The other two cases represent discharges where an n = 3 external field was applied to non-resonantly slow the rotation. The very low rotation outside of the q = 2.5 surface in discharges with n = 3 magnetic braking shows that rotation at the higher rational q surfaces is not required for passive RWM stability.

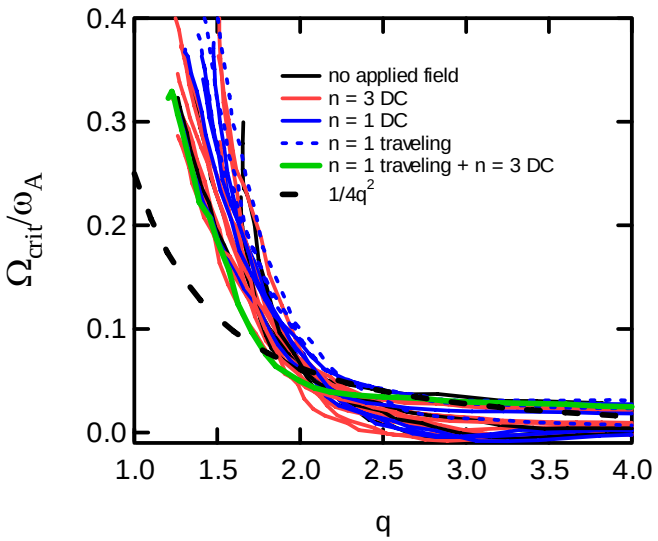

Fig. 4: Ω_{crit} profiles normalized to v_A showing significant variation across the entire profile.

A rapidly changing ω_ϕ increases the spread observed in Ω_{crit} profiles due to the 10 ms time resolution of the ω_ϕ measurement. The red dashed line shown in Fig. 3 represents the rotation profile preceding the red Ω_{crit} profile, which has strong magnetic braking giving the maximum change in ω_ϕ for one time step. The

Ω_{crit} profile database normalized to ω_A is shown in Fig. 4 and differentiated by the type of field applied for rotation braking. The maximum change in Ω_{crit}/ω_A at $q = 2$ during one time step as determined from Fig. 3 is 20% of the average of Ω_{crit}/ω_A at $q = 2$ in Fig. 4, while the Ω_{crit} spread at $q = 2$ in Fig. 4 is ±40%, consistent with Ω_{crit} being a profile rather than a scalar.

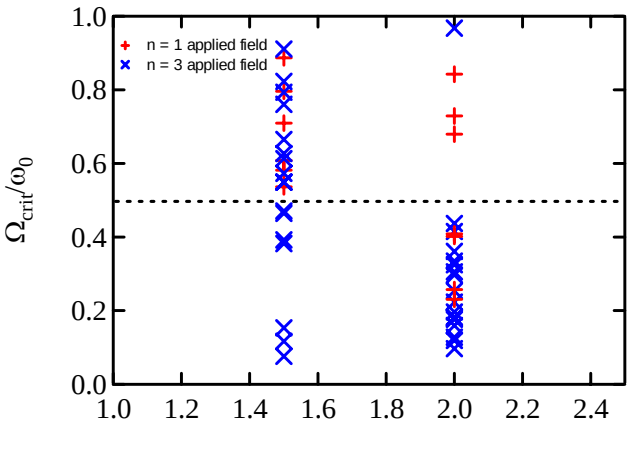

Fig. 5: Ω_{crit}/ω_0 at $q = 1.5$ & 2 showing stable plasmas at rotation lower than $\omega_0/2$.

The rapid decrease in rotation observed at RWM onset invites a comparison to the ”forbidden bands” of rotation caused by resonant MHD modes [19]. An electromagnetic torque model by Fitzpatrick [20] based on tearing mode interaction with a externally applied, non-axisymmetric field predicts a rotation bifurcation when rotation is slowed to one-half the steady-state value, ω_0, after which there is unstable mode growth and a rapid drop to zero rotation. The Ω_{crit} profile database (Fig. 5) shows the plasma to be stable at much lower rotation than $\omega_0/2$ at $q = 2$. The data further into the core at $q = 1.5$ also shows no correlation.

Shaing’s modification of the Fitzpatrick “simple” RWM model [21] includes neoclassical viscosity [22] and introduces a dependence on the ion collisionality, ν_{ii}, to the RWM dispersion relation. At low growth rate the viscous dissipation scales linearly with ν_{ii}, increased ν_{ii} is stabilizing and yields lower Ω_{crit}. A series of experiments were performed to examine the variation in Ω_{crit} with ν_{ii}. Comparing discharges with similar Alfvén speed, v_A, but varying ν_{ii} indeed shows increased ion collisionality leads to lower Ω_{crit}. This is shown in Fig. 6 where two discharges with varying collisionality but with constant q and v_A are compared. Throughout much of the cross section, v_A is nearly constant between the two discharges while ν_{ii} varies by nearly an order of magnitude, consistent with increased ν_{ii} leading to increased dissipation.

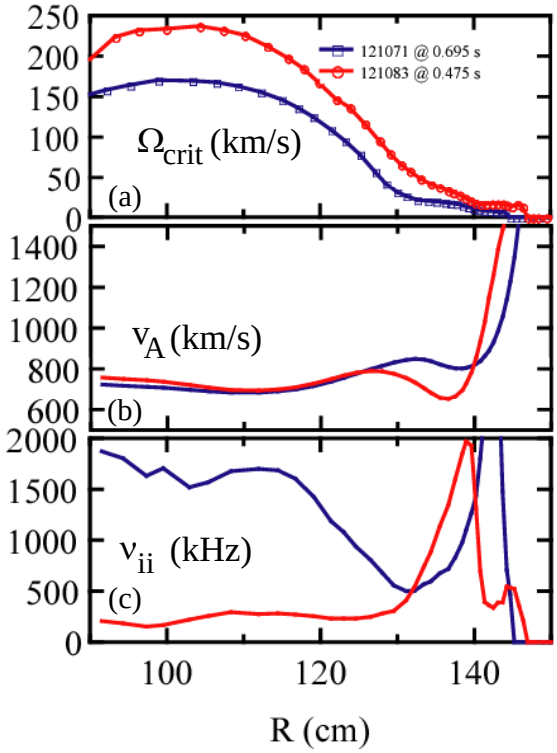

Fig. 6: Ω_{crit} variation with ν_{ii} for similar v_A cases showing lower critical rotation at higher ν_{ii}.

The RWM has also been observed to stabilize by an apparent seeding of other MHD modes. Normally, an unstable RWM will grow, further slowing plasma rotation, and cause discharge disruption. An example of this behavior is shown in Figs. 7 and 8. Fig. 7 shows the time evolution of (a) β_N (black trace) and the DCON [23] computed δw (dotted green), (b) the $n = 1$ perturbed B_p measured by the internal RWM sensors, and (c) an odd-n filtered toroidal Mirnov signal. The $\beta_N > \beta_N^{no\text{-}wall}$ leading up to the unstable mode growth as shown in Fig. 7(a). The RWM begins to grow just after 0.39s and reaches a peak δB_p at approximately 0.41s as shown in Fig. 7(b). After this time, the

RWM amplitude quickly drops as a more rapidly rotating internal mode grows as shown in Fig. 7(c). An examination of chordal USXR data from a midplane photodiode array shows the spatial extent of the two modes in Fig. 8. The inset area is shown in Fig. 8(b) where an $n = 1$ mode in the plasma interior is seen growing at 0.409s as the RWM begins to stabilize, preventing discharge disruption. This behavior is sometimes observed in high pressure discharges which are marginally stable to internal modes as computed by DCON.

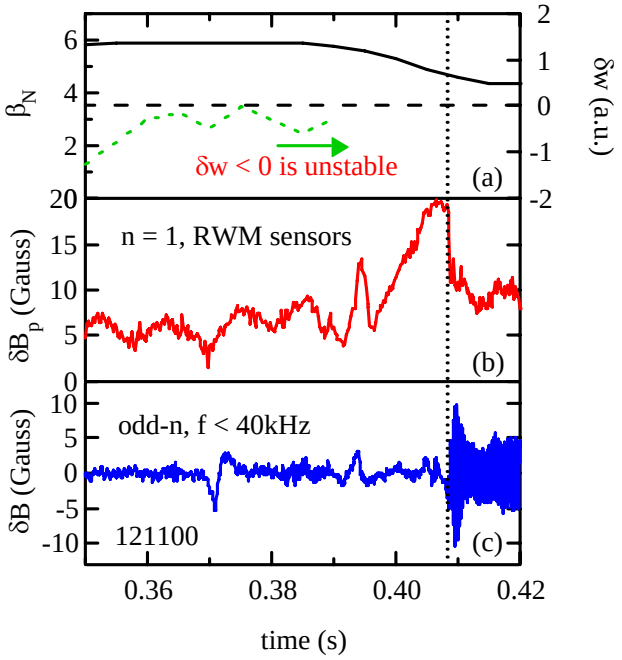

Fig. 7:Time evolution of (a) β_N (black solid) & DCON computed δw (green dashed), (b) the n = 1 component of δB_p measured by the internal RWM sensors, and (c) the odd-n filtered, low-f toroidal Mirnov signal.

5. Rotation Damping Physics

Non-axisymmetric fields were used to alter and reduce the plasma rotation by a non-resonant rotation damping mechanism that quantitatively agrees with neoclassical toroidal viscosity theory (NTV). [24]

Understanding of the physical mechanisms responsible for plasma momentum dissipation is needed to determine how the favorable plasma rotation can be sustained and maximized, or how the plasma rotation profile might be controlled in future tokamaks. This understanding of torque balance in high beta plasmas is also needed to accurately determine RWM stability and dynamics. While there has been success in understanding radially localized damping by tearing instabilities tied to rational magnetic surfaces [25,26] (resonant damping mechanisms), quantitative understanding of non-resonant momentum dissipation observed in experiments has been elusive.

Experimental comparison to theory has included semi-empirical application to tearing modes in DIII-D [27] and comparison to the plateau regime formulation using cylindrical approximations in JET [28] and NSTX [9]. The JET study found qualitative agreement to the measured global damping, but determined that the theory underestimated the observed damping by a few orders of magnitude. A more recent JET study discussed a rough estimate of the increase in NTV magnitude expected in the collisionless regime, showing the potential for greater agreement between theory and experiment [29]. In the present study, NTV theory appropriate for all collisionality regimes is

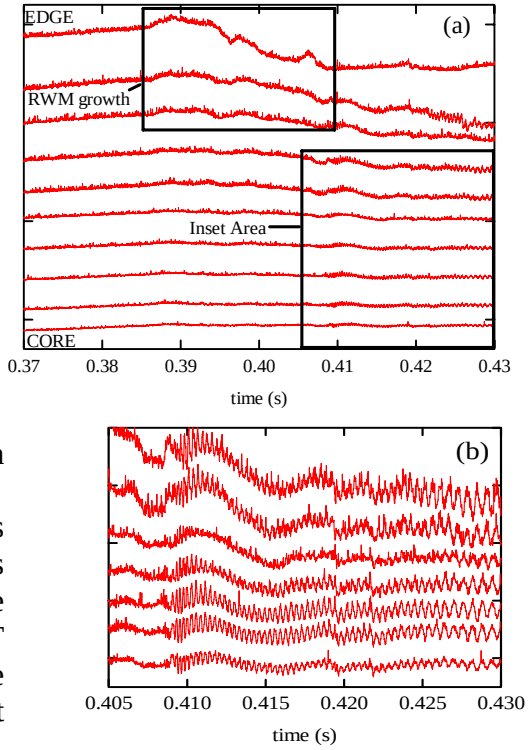

Fig. 8: SXR data showing (a) growth of RWM in edge channels and (b) subsequent internal mode.

quantitatively compared to experimental results. A significant conclusion of the present work is that theory and experiment agree to order one. Essential to this agreement is the inclusion of trapped particle effects and an accurate calculation of the applied field. [30]

The theoretical formulation of plasma toroidal momentum dissipation due to NTV was derived by Shaing, et al. for both the plateau and the collisional Pfirsch-Schluter transport regimes [24,31]. In the present study, the full formulation is used, and is computed in Hamada coordinates from experimental equilibrium reconstructions including magnetic pitch angle data from a motional Stark effect diagnostic. The complete set of equations used in the calculations can be found in Ref. [30] with the viscosity in the plateau and low collisionality regimes scaling as $\delta B^2 T_i^{0.5}$ and $\delta B^2 (T_i/\nu_i)(1/A)^{1.5}$, respectively. The change in the measured plasma angular momentum profile is compared to the theoretical NTV torque by evaluating the angular equation of motion $d(I\omega_\phi)/dt = \Sigma T_j$, where the torques exerted on equilibrium flux surfaces are due to: (i) neoclassical toroidal viscosity, T_{NTV}, (ii) momentum input due to high-power co-injected neutral beams, (iii) electromagnetic forces on rotating magnetic islands (resistive MHD modes), and (iv) fluid viscous forces between adjacent flux surfaces. I is the flux surface moment of inertia. The experimental procedure allows the isolation of the NTV torque, yielding $d(I\omega_\phi)/dt = T_{NTV}$, simplifying comparison of experiment to theory. [30]

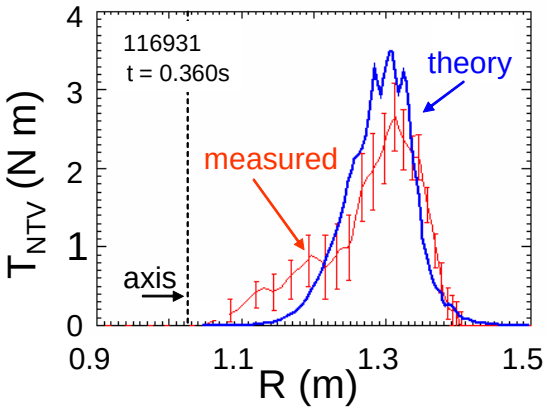

Fig. 9 Comparison of measured $d(I\omega_\phi)/dt$ profile to the theoretical integrated NTV torque for an n = 3 applied field

The plasma toroidal momentum dissipation is first evaluated at values of β_N below $\beta_N^{no\text{-}wall}$, the time evolution of which is evaluated by the DCON [23] ideal MHD stability code using experimental equilibrium reconstructions. When $\beta_N < \beta_N^{no\text{-}wall}$, RFA is measured to be insignificant. Comparison of the measured dissipation of plasma angular momentum caused by the externally-applied non-axisymmetric fields to the theoretical NTV torque profile is shown in Fig. 9 for an n = 3 applied field configuration. In this condition, NTV generated by n = 3 and 9 are most significant. [30] The measured value of $d(I\omega_\phi)/dt$ includes error bars that take into account the uncertainty in the measured ω_ϕ and mass density.

As β_N approaches and exceeds $\beta_N^{no\text{-}wall}$, RFA is measured as the applied non-axisymmetric field is amplified by the weakly-stabilized RWM and needs to be included in the calculation of T_{NTV}. The effect is most strongly observed when the non-axisymmetric coil is energized in an n = 1 configuration. In this condition, NTV generated by n = 1 and 5 are most significant. As the rotation decreases below Ω_{crit}, the n = 1 field grows more strongly and rapidly as the RWM becomes unstable. The RFA used in T_{NTV} is computed in two ways for comparison: (i) during early periods of RFA, the field is increased by multiplying the n = 1-3 components of the applied field by the measured RFA magnitude and (ii) during stronger RFA, or an unstable RWM, the field of the

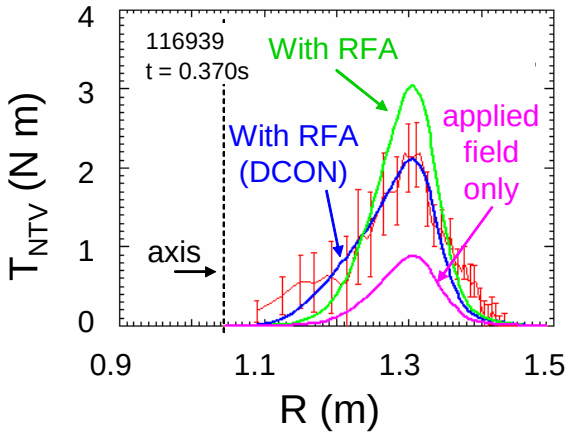

Fig. 10 Comparison of measured $d(I\omega_\phi)/dt$ profile to the theoretical integrated NTV torque during amplification of an n = 1 applied field configuration.

mode is modeled using the theoretical eigenfunction computed using DCON. The results using each technique are shown in Fig. 10, where T_{NTV} is also shown using the non-amplified applied field for comparison.

Similar analyses were conducted for thirty different equilibria with varying levels of non-axisymmetric field amplification. The ratio $(T_{NTV})/(d(I\omega_\phi)/dt)$ using the peak values along the radial profile for this ensemble of equilibria has a mean value of 1.59 with standard deviation of 0.87. This is significantly closer agreement than found in previous studies. The radial peak of the measured and computed profiles vary in alignment by 2.28 cm +/- 1.71 cm.

6. Conclusion

A non-asymmetric field coil has been added to NSTX to conduct RWM passive and active stabilization studies. The critical rotation speed for RWM stabilization more generally depends on the ω_ϕ profile shape, implying a radially distributed dissipation mechanism. The observed inverse dependence of Ω_{crit} on ν_{ii} indicates that plasmas at lower collisionality in ITER may require a higher degree of RWM active stabilization. A similar inverse dependence of plasma momentum dissipation on ν_{ii} in NTV theory further indicates that the ω_ϕ needed for RWM passive stability will be subject to higher viscosity and greater reduction. The strong δB^2 dependence of the quantitatively verified NTV theory also shows that error fields and their amplification by stable RWMs should be minimized to maximize ω_ϕ.

*Supported by US DOE Contracts DE-FG02-99ER54524 and DE-AC0276CH03073.

[1] ONO, M., KAYE, S.M., PENG, Y.-K.M., et al. Nucl. Fusion **40** (2000) 557.
[2] FREIDBERG, J.P., "Ideal Magnetohydrodynamics", Plenum Press, New York, (1987).
[3] BONDESON, A. and WARD, D.J., Phys. Rev. Lett. **72** (1994) 2709.
[4] TAYLOR, T.S., Phys. Plasmas **2** (1995) 2390.
[5] GAROFALO, A.M., JENSEN, T.H., and STRAIT, E.J., Phys. Plasmas **10** (2003) 4776.
[6] LIU, Y., BONDESON, A., CHU, M.S., et al., Nucl. Fusion **45** (2005)1131.
[7] SABBAGH, S.A., BELL, R.E., MENARD, J.E., et al., Phys. Rev. Lett. **97** (2006) 045004.
[8] SABBAGH, S.A., BELL, R.E., BELL, M.G., et al., Phys. Plasmas **9** (2002) 2085.
[9] SABBAGH, S.A., BIALEK, J.M., BELL, R.E., et al., Nucl. Fusion **44** (2004) 560.
[10] SABBAGH, S.A., SONTAG, A.C., BIALEK, J.M., et al., Nucl. Fusion **46** (2006) 635.
[11] SONTAG, A.C., SABBAGH, S.A., ZHU, W., et al., Phys. Plasmas **12** (2005) 056112.
[12] BOOZER, A.H., Phys. Rev. Lett. **86** (2001) 5059.
[13] REIMERDES, H., CHU, M.S., GAROFALO, A.M., et al., Phys. Rev. Lett. **93** (2004) 135002.
[14] BIALEK, J.M., BOOZER, A.H., MAUEL, M.E., et al., Phys. Plasmas **8** (2001) 2170.
[15] SABBAGH, S.A., KAYE, S.M., MENARD, J.E., et al., Nucl. Fusion **41** (2001) 1601.
[16] BETTI, R., FREIDBERG, J.P., Phys. Rev. Lett. **74** (1995) 2949.
[17] FITZPATRICK, R., AYDEMIR, A.Y., Nucl. Fusion, **36** (1996) 11.
[18] BONDESON, A., CHU, M.S., Phys. Plasmas **3** (1996) 3013.
[19] GATES, D.A., HENDER, T.C., Nucl. Fusion **36** (1996) 273.
[20] FITZPATRICK, R., Nucl. Fusion **33** (1993) 1061.
[21] FITZPATRICK, R., Phys. Plasmas **9** (2002) 3459.
[22] SHAING, K. C., Phys. Plasmas **11** (2004) 5525.
[23] GLASSER, A.H., CHANCE, M.C., Bull. Am. Phys. Soc. **42** (1997) 1848.
[24] SHAING, K.C., HIRSCHMAN, S.P., CALLEN J.D., Phys. Fluids **29** (1986) 521.
[25] SHAING, K.C., AYDEMIR, et al., Phys. Rev. Lett. **80** (1998) 5353.
[26] YOKOYAMA, M., CALLEN, J.D., HEGNA, C.C., et al., Nucl. Fusion **36** (1996) 1307.
[27] LA HAYE, R.J., GÜNTER, S., HUMPHREYS, D.A., et al., Phys. Plasmas **9** (2002) 2051.
[28] LAZZARO, E., BUTTERY, R.J., HENDER, T.C., et al., Phys. Plasmas **9** (2002) 3906.
[29] LAZZARO, E., ZANCA, P., Phys. Plasmas **10** (2003) 2399.
[30] ZHU, W., SABBAGH, S.A., BELL, R.E., *et al.*, Phys. Rev. Lett. **96** (2006) 225002.
[31] SHAING, K.C., Phys. Fluids B **5** (1993) 3841.